Carbohydrate Polymers 94 (2013) 584–593

Contents lists available at SciVerse ScienceDirect

Carbohydrate Polymers

journal homepage: www.elsevier.com/locate/carbpol

Biocompatibility and characterization of renewable agricultural residues and polyester composites

Chin-San Wu[a,*], Yi-Chiang Hsu[b], Jen-taut Yeh[c,d,e], Hsin-Tzu Liao[a], Jheng-Jie Jhang[a], Yong-Yu Sie[a]

[a] Department of Chemical and Biochemical Engineering, Kao Yuan University, Kaohsiung County, 82101, Taiwan, ROC
[b] Graduate Institute of Medical Science, and Innovative Research Center of Medicine, College of Health Sciences, Chang Jung Christian University, Tainan 71101, Taiwan
[c] Department of Materials Science and Engineering, National Taiwan University of Science and Technology, Taipei, Taiwan
[d] Department of Materials Engineering, Kun Shan University, Yung Kang, Tainan 71003, Taiwan, ROC
[e] Faculty of Chemistry and Material Science, Hubei University, Wuhan, Hubei, China

ARTICLE INFO

Article history:
Received 29 October 2012
Received in revised form
15 December 2012
Accepted 13 January 2013
Available online 4 February 2013

Keywords:
Composites
Poly(trimethylene terephthalate)
Sesame husk
Biocompatibility
Biodegradability

ABSTRACT

Composites of sesame husk and glycidyl methacrylate-grafted polytrimethylene terephthalate (PTT-g-GMA/SH) exhibit noticeably superior mechanical properties compared to PTT/SH composites due to greater compatibility between the two components. The dispersion of SH in the PTT-g-GMA matrix is highly homogeneous as a result of condensation reaction formations. Human lung fibroblasts (FBs) were seeded on these two series of composites to characterize the biocompatibility properties. In a time-dependent course, the FB proliferation results demonstrated higher performance from the PTT/SH series of composites than from the PTT-g-GMA/SH composites. In addition, collagen production by FBs present in the PTT/SH series was 20% higher than in regular culture-plates after 7 days of incubation. The water resistance of PTT-g-GMA/SH was higher than that of PTT/SH, although the weight loss of both composites buried in soil compost indicated that they were both biodegradable, especially at higher levels of SH substitution. The PTT/SH and PTT-g-GMA/SH composites were more biodegradable than pure PTT, implying a strong connection between SH content and biodegradability.

1. Introduction

Biomedical materials can be approximately divided into three major types: metals, ceramics, and organic plastic matter. Their derived products are used for different clinical applications (Golish & Anderson, 2012; Lévesque, Hermawan, Dubé, & Mantovani, 2008; Nair & Laurencin, 2007; Xuanyong, Chu, & Ding, 2010). For example, the various surgical instruments and internal and external fixing devices used in orthopedics are mostly made of metal, while ceramic material is mostly applied as a bone filling material. Organic plastic materials have been extensively developed into diversified, expendable medical products for 50 years due to their easy processability and good mechanical properties. Organic plastic materials have high biocompatibility and can transmit cell recognition signals, as well as be used for cell adsorption, multiplication, and differentiation (Brocchini, 2001; Shruti & John, 2011; You et al., 2010). Therefore, in addition to traditional medical appliances, organic plastic materials are presently being used in the development and application of tissue engineering materials. Tissue engineering aims to replace body parts that have impaired function due to diseases or injuries; it also aims to assist in wound healing, enhance the functions of organs and tissues, and rehabilitate or replace defective and abnormal tissues and organs (Artemenko et al., 2012; Marquès, Méndez, Gironès, Ginebra, & Pèlach, 2009). Furthermore, biomedical materials are expected to be emphasized in regenerative medicine in the future, and today's biomedical materials are mostly composed of organic plastic. To provide plastics with multiple functions, developing high quality aliphatic polyester plastics is very important. However, due to their typically poor mechanical properties, aliphatic polyester plastics have thus far only been used to develop nonelastic products [e.g., polylactic acid (PLA), polyhydroxybutyrate (PHB), polycaprolacton (PCL)]; in contrast, aromatic polyester plastics [e.g., polyethylene terephthalate (PET), polytrimethylene terephthalate (PTT), polybutylene terephthalate (PBT)], with their good mechanical properties and processability, can be extensively used to develop products meeting the market demand in tissue engineering and regenerative medicine. For these reasons, in this study, we investigated aromatic polyester plastics (Liu et al., 2005; Safapour et al., 2010).

PTT is a thermoplastic organic plastic typically formed by the reaction of 1,3-propanediol (1,3-PDO) with *N*,*N*′-dimethylaniline (DMA). This synthetic process saves more than 40% of the energy

* Corresponding author. Fax: +886 7 6077788.
E-mail address: t50008@cc.kyu.edu.tw (C.-S. Wu).

0144-8617/$ – see front matter © 2013 Elsevier Ltd. All rights reserved.
http://dx.doi.org/10.1016/j.carbpol.2013.01.083

used in traditional petroleum extraction methods for PTT production, and the PTT material can be recovered completely, thus reducing the consumption of both raw materials and energy. In addition, the formation of the toxic by-product acrolein can be reduced by more than 95% compared to traditional PTT formation methods; hence, PTT today is regarded as an environmentally friendly, recycled material with zero pollution. PTT is characterized by elasticity, ductility, flexibility, and minimal deformability. It also has a positive effect on the fiber structure of green products through special processing, imparting such products with antistatic properties, ultraviolet resistance, chlorine resistance, and fouling resistance, without any chemical treatment (Gupta & Choudhary, 2012; Toshikazu, Barbara, & Akio, 2012). In the past decade, several companies have paid close attention to this topic and have investigated how to improve the durability and practicability of this polyester. Unfortunately, PTT does not typically provide economic benefits; it has a relatively high cost, and thus agricultural residues [e.g., rice husk, bamboo and sesame husk (SH)] have been added to the PTT plastic as a filling material to reduce its cost (Nyambo, Mohanty, & Misra, 2010; Sain & Panthapulakkal, 2006).

In this study, we evaluated sesame husk as filling material for PTT. Sesame husk is a type of vegetable fiber that contains large amounts of vitamins B_1, B_2, B_6, C, and E, as well as dietary fiber. The main constituent is vitamin E, which is regarded as an antiaging vitamin that can be effective for improving blood circulation and promoting metabolism. In addition to the above-mentioned nutrients, sesame husk contains vegetable compounds, including polyphenols such as anthocyanin, lignin, and vitamin B_1, all of which can improve immunity and anti-oxidation effects, inhibit cancer cell multiplication (e.g., mastocarcinoma and skin carcinoma), and enhance cell vitality, thus making cells unlikely to cancerate (Mohdaly, Smetanska, Ramadanc, Sarhan, & Mahmoud, 2011; Sain & Panthapulakkal, 2006; Suja, Abraham, Thamizh, Jayalekshmy, & Arumughan, 2004; Suja, Jayalekshmy, & Arumughan, 2005).

This report describes a systematic investigation of the biocompatibility, mechanical and thermal properties, and biodegradability of SH composites with PTT and glycidyl methacrylate-grafted poly(trimethylene terephthalate) (PTT-g-GMA). The biocompatibility of composites was characterized using a cytotoxicity assay, cell surface adhesion, and the soluble collagen assay. The results of this study will be applicable to the development of biomedical materials and serve as a reference for future-developed biomedical composites.

2. Experimental

2.1. Materials

PTT was supplied by Shell Chemical Co. (Singapore); glycidyl methacrylate (GMA), benzoyl peroxide (BPO), and dimethyl sulfoxide (DMSO) were purchased from Sigma–Aldrich Chemical Inc. (St. Louis, MO, USA). 3-(4,5-Dimethylthiazol-2-yl)-2,5-diphenyltetrazoleliumbromide (MTT) was obtained from Promega (Madison, WI, USA). Fetal bovine serum (FBS) and Dulbecco's modified Eagle's medium (DMEM) were purchased from Gibco-BRL (Gaithersburg, MD, USA). All buffers and other reagents were of the highest purity commercially available. SH was obtained from Tainan (Taiwan).

2.2. Preparation and testing of PTT/SH composites

2.2.1. PTT-g-GMA copolymer

The grafting reaction of GMA onto PTT is illustrated in Scheme 1(A). A mixture of GMA and benzoyl peroxide was added in four equal portions at 2-min intervals to molten PTT to allow grafting to take place. The reactions were performed in a nitrogen (N_2) atmosphere at $45 \pm 2\,^{\circ}C$. Preliminary experiments showed that reaction equilibrium was attained in less than 12 h. Thus, reactions were allowed to progress for 12 h under stirring at 60 rpm. The product (4 g) was dissolved in 200 mL of refluxing phenol/tetrachloroethane solution (60:40 v/v) at $40 \pm 2\,^{\circ}C$, and then the solution was filtered through several layers of cheesecloth. The phenol/tetrachloroethane-soluble product in the filtrate was extracted five times using 600 mL of cold acetone per extraction. The GMA loading of the phenol/tetrachloroethane-soluble polymer was determined by titration and expressed as a grafting percentage as follows. Approximately 2 g of copolymer was heated for 2 h in 200 mL of refluxing phenol/tetrachloroethane solution. After the sample was completely dissolved, 0.8 mL of hydrogen chloride in 5 mL diethyl ether (1.0 M) was added to open the epoxide rings of PTT-g-GMA. Then, the excess hydrogen chloride (HCl) was titrated with 0.05 M methanolic sodium hydroxide (NaOH) solution using a phenolphthalein indicator. The grafting percentage was calculated using the following equations (Cho, Eom, Kim, & Park, 2008):

$$\text{Grafting percentage (wt\%)} = \frac{(0.6 \times 10^{-3} - 0.05 \times 10^{-3} V_s) \times 142.15\ \text{g/mol}}{2} \times 100, \quad (1)$$

where V_S is the volume of NaOH solution for titration (mL) and 142.15 g/mol is the molecular weight of GMA. The grafting yield was 2.11 wt% for BPO and GMA loadings of 0.3 and 10 wt%, respectively.

2.2.2. SH processing

SH was extracted as a by-product of sesame husk processing from 4 to 6 months and was supplied by Tainan of Taiwan. As shown in Scheme 1(B), purification consisted of immersing 60 g ground and dried SH in 1000 mL distilled water for 2 days to remove any water-soluble components. The product was then dried at 50–60 °C for 2 days under vacuum. The resulting brown fragments were 0.1–0.5 cm long. The fibers were dried, ground, and sorted. After grinding, the fiber mixture consisted of a fine brown powder. The samples were passed through 300-mesh and 400-mesh sieves, air-dried for 2 days at 50–60 °C, and vacuum-dried for at least 6 h at 100–110 °C until the moisture content fell to $5 \pm 2\%$.

2.2.3. Composite preparation

Prior to composite fabrication, SH samples were cleaned with acetone and dried in an oven at 105 °C for 24 h. Composites were prepared in a Plastograph® 200-Nm mixer W50EHT with a blade rotor (Brabender, Dayton, OH, USA). The blends were mixed between 220 °C and 230 °C for 20 min at a rotor speed of 50 rpm. Composite samples were prepared with SH:PTT or SH:PTT-g-GMA mass ratios of 10/90, 20/80, 30/70, and 40/60. Residual GMA in the PTT-g-GMA reaction mixtures was removed via acetone extraction prior to the preparation of PTT-g-GMA/SH composites. After mixing, the composites were pressed into thin plates using a hot press and placed in a dryer for cooling. These thin plates were cut to standard sample dimensions for further characterization.

2.2.4. Characterization analyses

The composites were characterized using Fourier-transform infrared spectroscopy (FTIR) and ^{13}C nuclear magnetic resonance (NMR) to identify bulk structural changes induced by the maleic anhydride moiety. Solid-state ^{13}C NMR was performed using an AMX-400 NMR spectrometer (Bruker, Billerica, MA, USA) and was obtained at 100 MHz under cross-polarization while spinning at the magic angle. Power decoupling conditions were set with a 90° pulse and a 4-s cycle time. Infrared spectra of the samples were obtained using an FTS-7PC FTIR spectrophotometer (Bio-Rad, Hercules, CA,

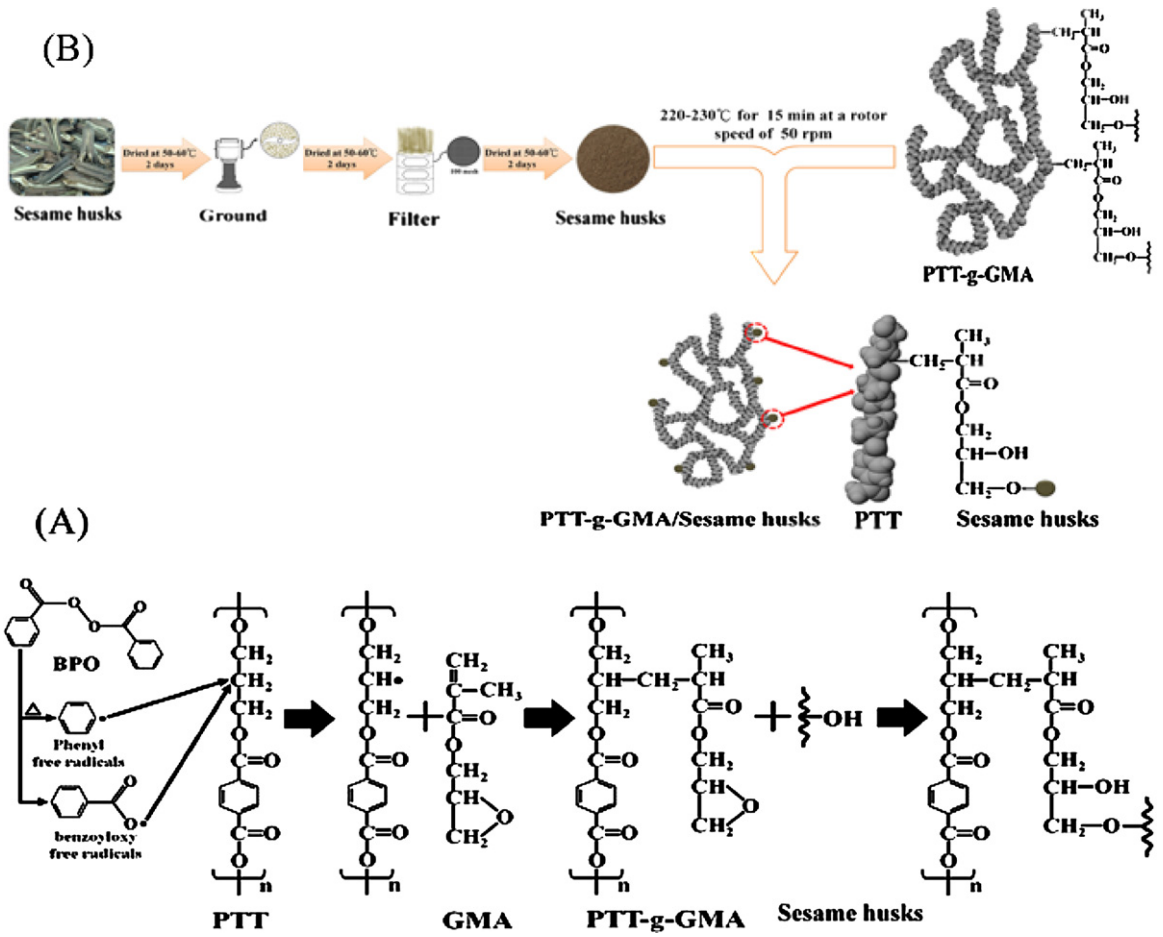

Scheme 1. (A) The grafting reaction of GMA onto PTT. (B) Modification of PTT with agricultural residues (sesame husks, SH) and the preparation of composite materials.

USA). A mechanical tester (model LLOYD, LR5K type; Instron, Norwood, MA, USA) was used to measure the tensile strength and the elongation at break in accordance with ASTM D638. Test samples were prepared in a hydrolytic press at 230 °C and conditioned at 50 ± 5% relative humidity (RH) for 24 h before making measurements. Measurements were made using a crosshead speed of 20 mm/min. Five measurements were performed for each sample, and the mean value was determined. The glass transition temperatures (T_g), melting temperatures (T_m), and heat of fusion (ΔH_f) were determined with a differential scanning calorimeter (DSC; model 2010 DSC; TA Instruments, New Castle, DE, USA). Sample quantities ranged from 4 to 6 mg; melting curves were recorded between 0 °C and 300 °C at a heating rate of 10 °C per min. Values of T_g, T_m, and ΔH_f were extracted from the temperatures and areas of melting peaks in the DSC heating thermograms. A thin film (150 mm × 150 mm × 1 mm) of each composite was prepared with a hydraulic press and treated with hot water at 60 °C for 24 h. Specimens were cut according to ASTM D638. After rupture, a thin section of the fracture plane was removed. The thin sections were then coated with gold, and the fracture surface morphologies were observed using a scanning electron microscope (SEM; model S-1400; Hitachi Microscopy, Tokyo, Japan).

2.3. Bio-functions of human lung fibroblasts on the PTT series composites

2.3.1. Cell and culture medium

Human lung fibroblasts (FBs, MRC-5) were supplied by the Bioresource Collection and Research Center in Taiwan. The MRC-5 cells were grown in culture medium [90% Eagle's minimum essential medium (EMEM) with 2 mM L-glutamine and Earle's balanced salt solution (EBSS) adjusted to contain 1.5 g/L sodium bicarbonate, 0.1 mM nonessential amino acids, and 1.0 mM sodium pyruvate + 10% FBS]. The cells were cultivated at 37 °C in a humidified incubator with a 5% CO_2 atmosphere.

2.3.2. Cell viability assay

The MTT assay (Su, Lin, Lee, & Ho, 2005) was used to evaluate the cytotoxicities of human lung FB cells on the membranes. The sample sheets were contained in 24-well plates and sterilized by ultraviolet light for 1 h. Each well plate was embedded with 5×10^4 human lung FBs, which were incubated with 5% CO_2 at 37 °C for 1, 4, and 7 days, respectively. At the end of the incubation period, the media in the plates was discarded, and the cells were washed once with phosphate-buffered saline (PBS). Each well plate was then filled with 100 μL of MTT in a dark environment. The culture was incubated for 4 h to convert the MTT to formazan. The supernatant was then removed, and 150 μL of the DMSO solution was added to dissolve the formazan. The plates were shaken and stirred to ensure the formation of a uniform solution, and the optical density (OD) was read at 540 nm.

2.3.3. Collagen quantification

The composite material sheets were contained in 24-well plates and sterilized by ultraviolet light for 1 h. The well plates were then embedded with 3×10^4–5×10^4 human lung FB cells, which were incubated with 5% CO_2 at 37 °C for 24 h. A total of 0.1 mL of the culture fluid from the samples and 1 mL of Sircol dye reagent were

mixed in a centrifuge tube for 1 h. The mixed liquid was centrifuged under 12,000 × *g* for 10 min. The supernatant was then removed, and the residual liquid on the edge of the centrifuge tube was removed using absorbent paper. It was necessary to avoid touching the precipitate during the process. Next, 1 mL of an alkali reagent was added to dissolve the precipitate, and after 10 min of stable coloration, 0.2 mL was extracted to 96-well plates. The stain was placed into the 96-well plates, and the absorbance was read at 540 nm using a spectrometer plate reader.

2.4. Water absorption

Samples were prepared for water absorption measurements by cutting the composites into 50 × 30-mm strips (150 ± 5 μm thickness) in accordance with ASTM D570. The samples were dried in a vacuum oven at 50 ± 2 °C for 8 h, cooled in a desiccator, and then immediately weighed to the nearest 0.001 g. This weight was designated W_c. Thereafter, the samples were immersed in distilled water and maintained at 25 ± 2 °C for a 60-day period. During this time, they were removed from the water at 10-day intervals, gently blotted with tissue paper to remove excess water from their surfaces, immediately weighed to the nearest 0.001 g three times, and then returned to the water. An average value of the weight measured at each 10-day interval was calculated, and these average weights were designated W_w. The percentage of weight increase due to water absorption (W_f) was calculated to the nearest 0.01% according to Eq. (2):

$$\%W_f = \frac{W_w - W_c}{W_c} \times 100\%. \quad (2)$$

2.5. Biodegradation studies

Biodegradability of the samples was assessed by measuring the weight loss of the composites over time in soil. Samples measuring 50 mm × 30 mm × 1 mm were weighed and buried in boxes containing alluvial-type soil obtained from farmland topsoil before planting. The soil was sifted to remove large clumps and plant debris. Soil was maintained at approximately 35% moisture by weight, and the samples were buried at a depth of 12–15 cm. A control box consisted of samples and no soil. The samples were unburied after 20 days, washed in distilled water, dried in a vacuum oven at 50 ± 2 °C for 3 days, and equilibrated in a desiccator for at least 1 day. The samples were then weighed before being returned to the soil.

2.6. Statistical analysis

Results are presented as a mean value of the data obtained from triplicate experiments. Student's *t*-test was used to determine the level of significance. Differences were considered nonsignificant when $P > 0.05$, significant when $P \leq 0.05$, and very significant when $P \leq 0.01$.

3. Results and discussion

3.1. Structure of PTT and its composites

FTIR spectroscopy was used to examine the grafting of GMA onto PTT. The FTIR spectra of PTT and PTT-*g*-GMA are shown in Fig. 1A andB. Characteristic peaks for PTT at 3200–3700, 1700–1750, and 500–1600 cm^{-1} appeared in both polymers (Yao & Yang, 2010). Two extra shoulders characteristic of ester carboxyl groups were observed at 1730 cm^{-1} in the modified PTT-*g*-GMA spectrum. Similar results have been reported previously (Cartier & Hu, 1998; Torres, Robin, & Boutevin, 2001). The shoulders represent free acid

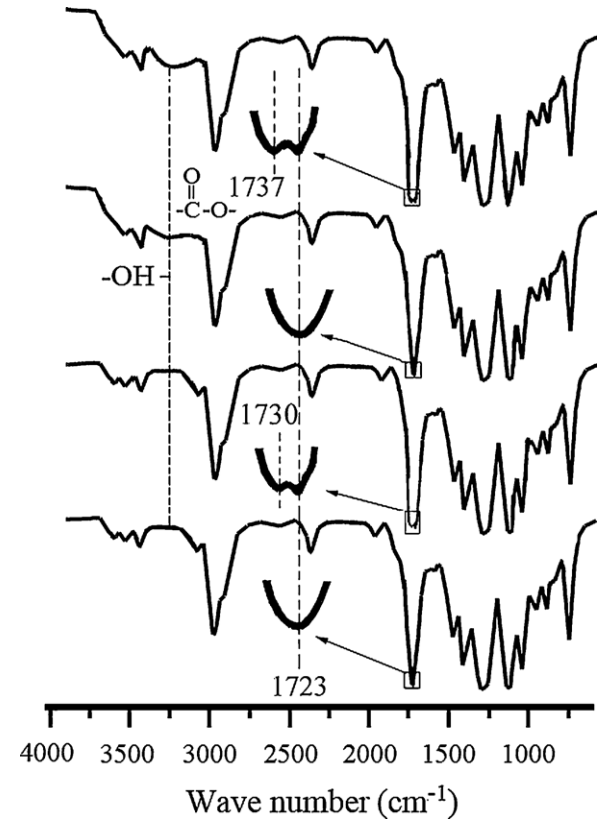

Fig. 1. FTIR spectroscopy spectra for (A) PTT, (B) PTT-g-GMA, (C) PTT/SH (20 wt%), and (D) PTT-g-GMA/SH (20 wt%).

in the modified polymer PTT-*g*-GMA and thus indicated the successful grafting of GMA onto PTT.

In the composite PTT/SH (20 wt%), the peak assigned to the O—H stretching vibration at 3200–3700 cm^{-1} intensified (Fig. 1C) due to contributions from the –OH group of SH. The FTIR spectrum of the PTT-g-GMA/SH (20 wt%) composite in Fig. 1D revealed a peak at 1737 cm^{-1} that was not present in the FTIR spectrum of the PTT/SH (20 wt%) blend. This peak was assigned to the ester carbonyl stretching vibration of the copolymer. Kocer et al. also reported an absorption peak at 1737 cm^{-1} for this ester carbonyl group (Kocer, Cerkez, Worley, Broughton, & Huang, 2011). These spectral data suggest the formation of branched and cross-linked macromolecules in PTT-g-GMA/SH by covalent reaction of the glycidyl methacrylate groups in PTT-g-GMA with the hydroxyl groups of SH.

Further evidence of ester formation was provided by ^{13}C solid-state NMR spectroscopy. The ^{13}C solid-state NMR spectrum of neat PTT (Fig. 2A) was similar to that reported by Kameda, Miyazawa, and Murase (2005) and showed five peaks: (1) $\delta = 27.8$ ppm, (2) $\delta = 62.6$ ppm, (3) $\delta = 129.8$ ppm, (4) $\delta = 133.7$ ppm, and (5) $\delta = 165.5$ ppm). Compared with that of neat PTT, the ^{13}C solid-state NMR spectrum of PTT-g-GMA (Fig. 2B) contained three additional peaks: (6) $\delta = 19.2$ ppm, (7) $\delta = 54.8$ ppm, (8) $\delta = 50.2$ ppm, (9) $\delta = 175.6$ ppm, (10) $\delta = 68.3$ ppm, and (11, 12) $\delta = 45.6$ ppm. These peaks confirmed the grafting of GMA onto PTT, as illustrated in Fig. 2B.

The solid-state ^{13}C NMR spectra of PTT-g-GMA/SH (20 wt%), PTT/GMA (20 wt%), and SH are shown in Fig. 2C–E. The spectra are similar to those reported by Kuo, Lin, Chen, Yiu, & Tzen (2011). Relative to unmodified polyester, additional peaks were observed in the spectra of composites containing PTT-g-GMA. These additional peaks were located at (6)–(12). These same features were observed

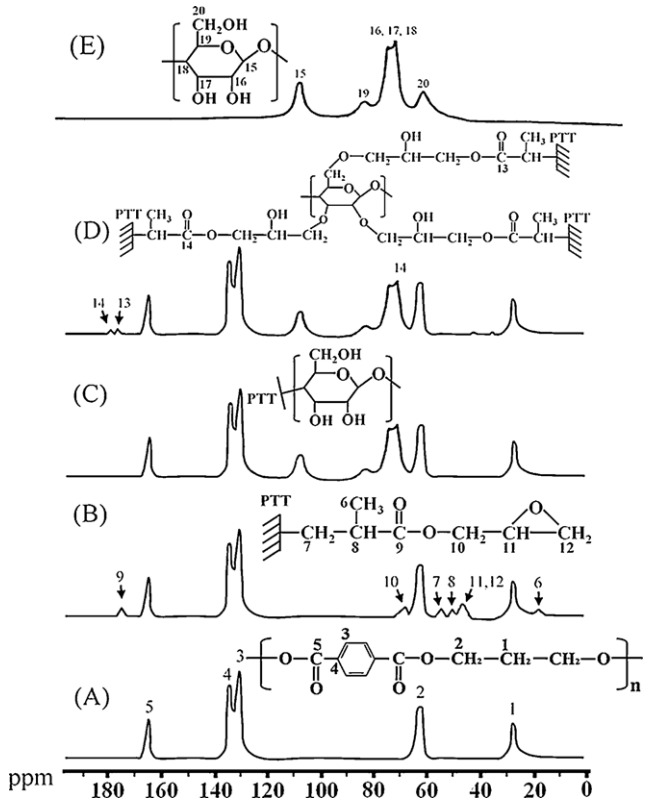

Fig. 2. Solid-state ^{13}C NMR spectra for (A) PTT, (B) PTT-g-GMA, (C) PTT/SH (20 wt%), (D) PTT-g-GMA/SH (20 wt%), and (E) SH.

in previous studies (Juntuek, Ruksakulpiwat, Chumsamrong, & Ruksakulpiwat, 2011) and indicate grafting of GMA onto PTT. However, the peak at δ = 175.6 ppm (C=O) (9) (Fig. 2B), which is also typical for GMA grafted onto PTT, was absent in the solid-state spectrum of PTT-g-GMA/SH (20 wt%). This absence is most likely a result of an additional condensation reaction between the glycidyl methacrylate group of GMA and the –OH group of SH that caused the peak at δ = 175.6 ppm to split into two bands (δ = 176.9 and 178.3 ppm). This additional reaction converted the fully acylated groups in the original SH to esters (represented by peaks 13 and 14 in Fig. 2C) and did not occur between PTT and SH, as indicated by the absence of corresponding peaks in the FTIR spectrum of PTT/SH (20 wt%) in Fig. 2D. The formation of ester groups significantly affects the mechanical properties of PTT-g-GMA/SH and is discussed in greater detail in the following sections.

3.2. Morphology and mechanical properties of PTT and its composites

In most composite materials, effective wetting and uniform dispersion of all components in a given matrix and strong interfacial adhesion between the phases are required to obtain a composite with satisfactory mechanical properties. In the current study, SH may be thought of as a dispersed phase within a PTT or-PTT-g-GMA matrix. To evaluate the composite morphology, SEM was employed to examine tensile fractures in the surfaces of PTT/SH (20 wt%) and PTT-g-GMA/SH (20 wt%) samples. The SEM microphotograph of PTT/SH (20 wt%) in Fig. 3A shows that the SH fibers in this composite tended to exhibit poor interfacial adhesion in the matrix. This poor interfacial adhesion was due to the formation of hydrogen bonds between SH and the disparate hydrophilicities of PTT and SH. Poor wetting in these composites was also noted (Fig. 3A) due to large differences in surface energy between the SH

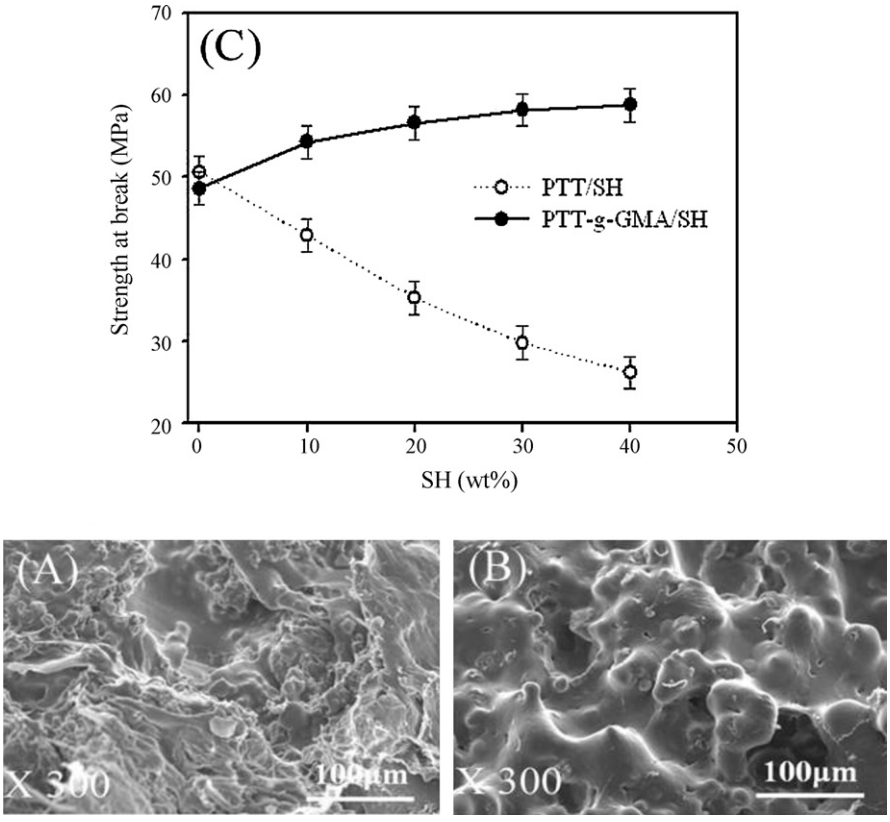

Fig. 3. SEM photomicrographs showing the distribution and adhesion of SH in (A) PTT/SH (20 wt%) and (B) PTT-g-GMA/SH (20 wt%) composites. (C) The effect of SH content on tensile strength at break is shown for PTT/SH and PTT-g-GMA/SH composites.

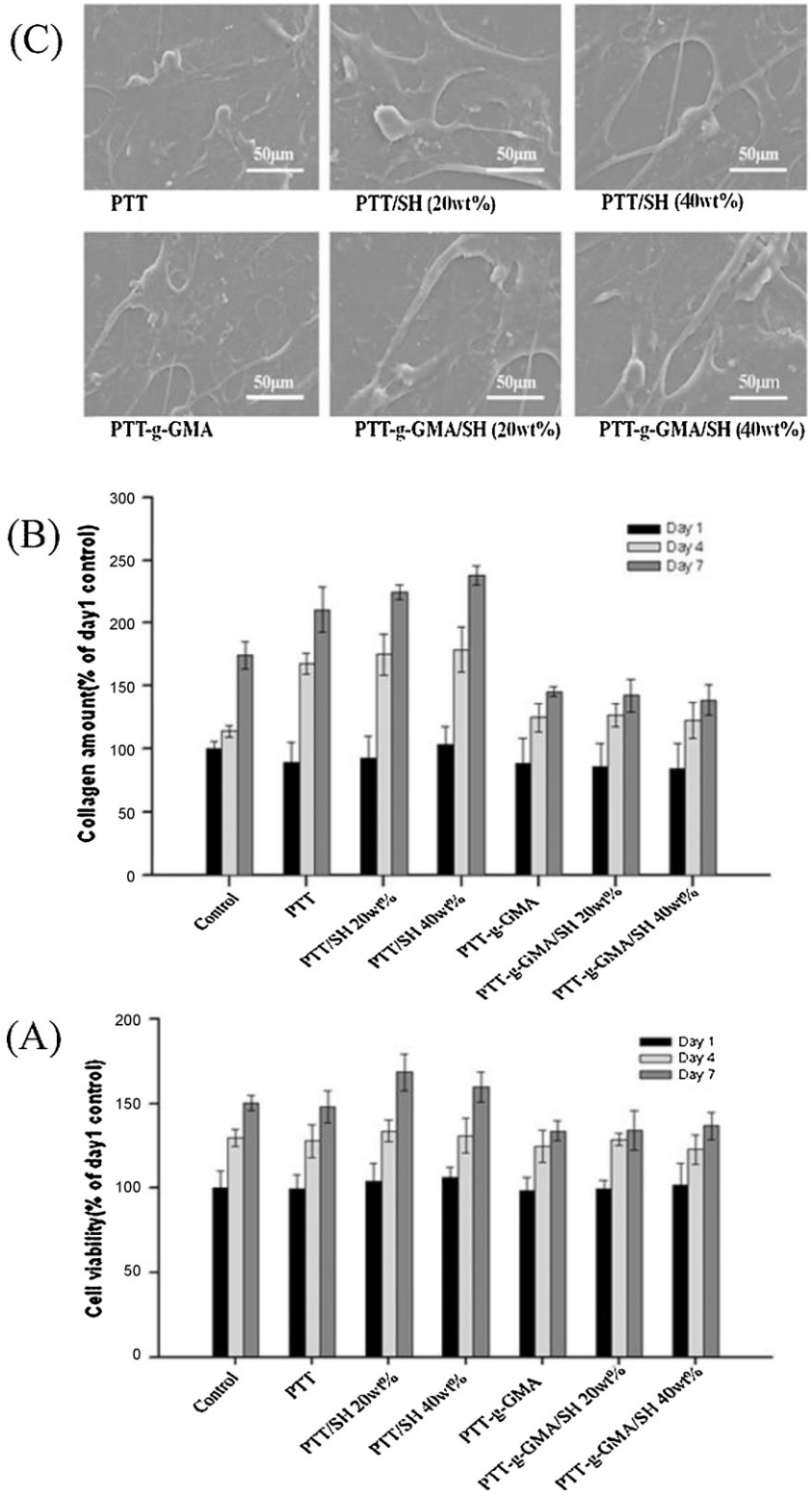

Fig. 4. (A) Cell proliferation ratios of human lung FBs seeded on two series membranes. From 1 to 7 days, the cell proliferation rate was quantified by MTT assay. (B) The collagen amount secreted from human lung FBs seeded on two series membranes for 7 days. Sircol dye was used to quantify the collagen amount. (C) SEM micrographs of human lung FBs and collagen on the PTT, PTT/SH, and PTT-g-GMA/SH membranes after 7 days of culture (scale bar is 50 μm).

and the PTT matrix (Wong, Zahi, Low, & Lim, 2010). In contrast, the PTT-g-GMA/SH (20 wt%) microphotograph presented in Fig. 3B shows a more homogeneous dispersion and better wetting of SH in the PTT-g-GMA matrix, as indicated by the complete coverage of PTT-g-GMA on the fiber and the removal of both materials when a fragment was pulled from the bulk. This improved interfacial adhesion is due to the similar hydrophilicity of the two components, which allows for the formation of branched and cross-linked macromolecules, and the prevention of hydrogen bonding between SH composites.

Table 1
Influence of SH content on the thermal properties of PTT/SH and PTT-g-GMA/SH composites.

SH	PTT/SH			PTT-g-GMA/SH		
(wt%)	T_g (°C)	T_m (°C)	ΔH_f (J/g)	T_g (°C)	T_m (°C)	ΔH_f (J/g)
0	54.3	229.3	55.6	53.2	227.6	54.1
10	55.1	226.8	47.8	59.6	225.8	52.6
20	56.2	225.6	43.6	62.3	223.2	51.5
30	57.1	225.0	41.5	63.5	222.7	50.9
40	57.9	224.6	40.1	64.6	222.3	50.5

Fig. 3C shows the variation in tensile strength at break with SH content for the two composites. The tensile strength of pure PTT (56.6 MPa) decreased after grafting with GMA (48.6 MPa). That of PTT/SH composites (Fig. 3C) decreased markedly and continuously with increasing SH content (from 50.68 to 26.2 MPa). This decrease was attributable to poor dispersion of SH in the PTT matrix, according to the morphology discussed previously and as shown in Fig. 3A. The effect of this incompatibility on the mechanical properties of the composites was substantial. The PTT-g-GMA/SH composites shown in Fig. 3C exhibited unique behavior; tensile strength at break decreased with increasing SH content despite the fact that PTT-g-GMA had a lower tensile strength than pure PTT. Furthermore, the tensile strength of the PTT-g-GMA/SH composites remained constant or slowly increased with SH content greater than 20 wt%, likely due to the enhanced dispersion of SH in the PTT-g-GMA matrix resulting from the formation of branched or cross-linked macromolecules (Kuan, Ma, Kuan, Wu, & Liao, 2006). In addition, the tensile strength of PTT-g-GMA/SH was approximately 11–23 MPa higher than that of PTT/SH.

3.3. Thermal properties of PTT and its composites

The ΔH_f, T_m, and T_g of both PTT/SH and PTT-g-GMA/SH composites with various SH contents were determined by measuring DSC heating thermograms (Table 1). For both composites, T_m decreased with increasing SH content. This decrease in T_m may have been due to the inclusion of SH in the composites; SH will expand PTT or PTT-g-GMA, hence causing slack polymer structure and reduced T_m. At the same SH content, the PTT/SH composites had a higher T_m than the PTT-g-GMA/SH composites. The T_g increased with increasing SH content for both PTT/SH and PTT-g-GMA/SH composites. This increase was likely a result of decreasing space available for molecular motion. T_g values were higher for the PTT-g-GMA composites by between 1.0 °C and 8.5 °C, suggesting that the grafting of glycidyl methacrylate groups to the PTT further restricted molecular motion.

The ΔH_f of pure PTT was 55.6 J/g, whereas that of PTT-g-GMA was 54.1 J/g (Table 1). The lower ΔH_f of PTT-g-GMA was attributable to the disruption of regularity in chain structure and increased spacing between chains as a result of the grafted branches. The values of ΔH_f in PTT-g-GMA/SH were approximately 2–11 J/g higher than those in PTT/SH. These higher ΔH_f values were attributable to the formation of ester carbonyl groups as discussed above. The ΔH_f may be used as an indicator of blend crystallinity. Although ΔH_f of both PTT/SH and PTT-g-GMA/SH blends decreased with increased SH content (Table 1), the extent of the decrease was significantly greater in PTT/SH, indicating a lower degree of crystallinity. These results are similar to those obtained elsewhere with composites of PTT and agricultural residues (Wu, 2011). The marked decrease in the crystallinity of PTT/SH was attributable to hindered motion of the PTT polymer segments as a result of the presence of SH in the composite matrix (Wong, Shanks, & Hodzic, 2004).

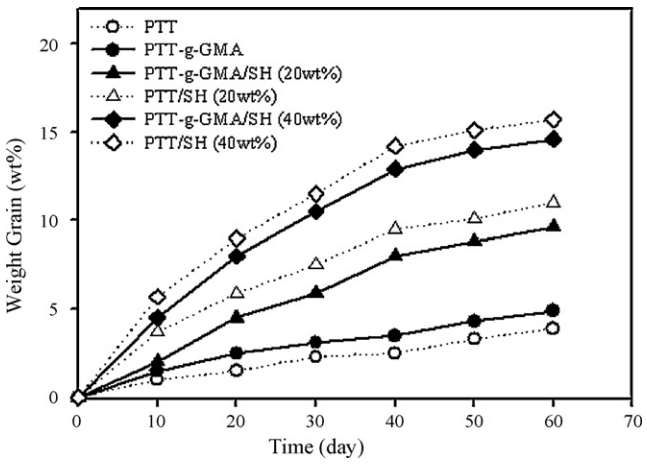

Fig. 5. Percent weight gain due to the absorption of water for PTT/SH and PTT-g-GMA/SH composites.

3.4. Biocompatibility properties of PTT and its composites

The composites' biocompatibility was evaluated by measuring the cell growth rate of human lung FBs seeded on the membranes (Fig. 4). The cell viability was examined by MTT assay. The FB cell numbers on different membranes were measured (Fig. 4A). Upon seeding of FBs on the membranes, the PTT/SH series membranes showed similar cell viabilities to FBs seeded on the plate directly from the 1st day to the 7th day, which revealed that the membranes have good compatibility with human lung FBs. With increasing SH content, the cell viability did not exhibit obvious differences; at SH contents of 10 and 30 wt%, the results were similar (data not shown). The FB cell viabilities on PTT-g-GMA membranes were slightly lower than on the plate on the 1st day. However, on the 7th day, the cell viabilities were quite similar to those observed for the PTT/SH series and on the plate.

Sircol dye was used to stain the collagen secreted by human lung FBs on the well or on the membranes. In Fig. 4B, which compares the seeding of FBs on the plates, the collagen production on different membranes was similar at day 1. At day 4 or 7, collagen production by human lung FBs on PTT/SH was higher than on the plate, the vehicle control. With increasing SH content, the collagen production increased. Less collaged was produced in the PTT-g-GMA series than in the PTT series but also more than in the control on day 4. On day 7, the collagen amount produced on the PTT series membranes increased. These results indicated that PTT series membranes stimulated collagen secretion in the FBs.

Collagen is an important component for cell proliferation and tissue body formation, which are dependent on FB production (Kim, Chun, Han, & Kim, 2010). Collagen in extracellular matrix (ECM) imparts appropriate mechanical strength to the tissue body shape (Muzzarellia, Grecoa, Busilacchia, Sollazzob, & Gigantea, 2012; Sell, McClure, Garg, Wolfe, & Bowlin, 2009). Therefore, the concentration of collagen secreted is a key indicator of biocompatibility. Because the PTT series membranes stimulated collagen secretion by FBs, these membranes may be good biomaterials for tissue engineering. Fig. 4C shows the SEM image of collagen and FBs on cell-treatment membranes (7 days). The arrows indicate the adhesion of collagen. With increasing SH contents in PTT, more excretion of collagen was observed in the SEM image; these results indicated that the membranes could stimulate collagen production.

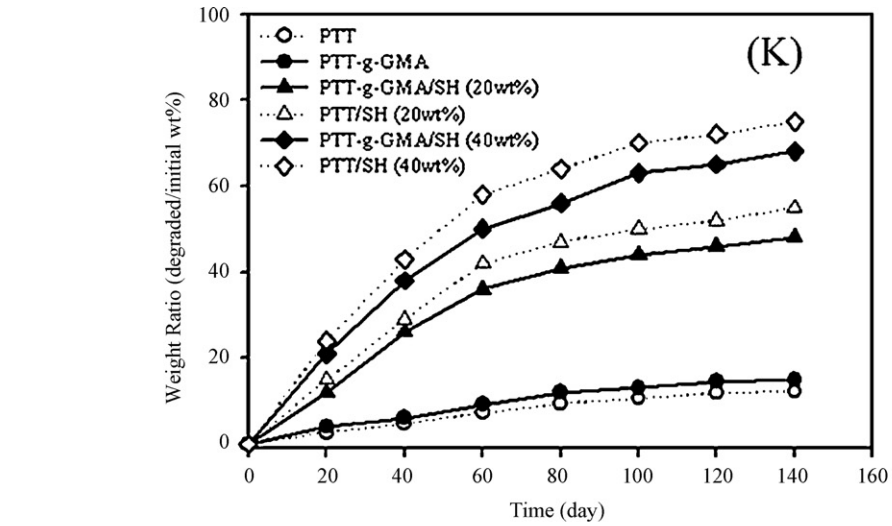

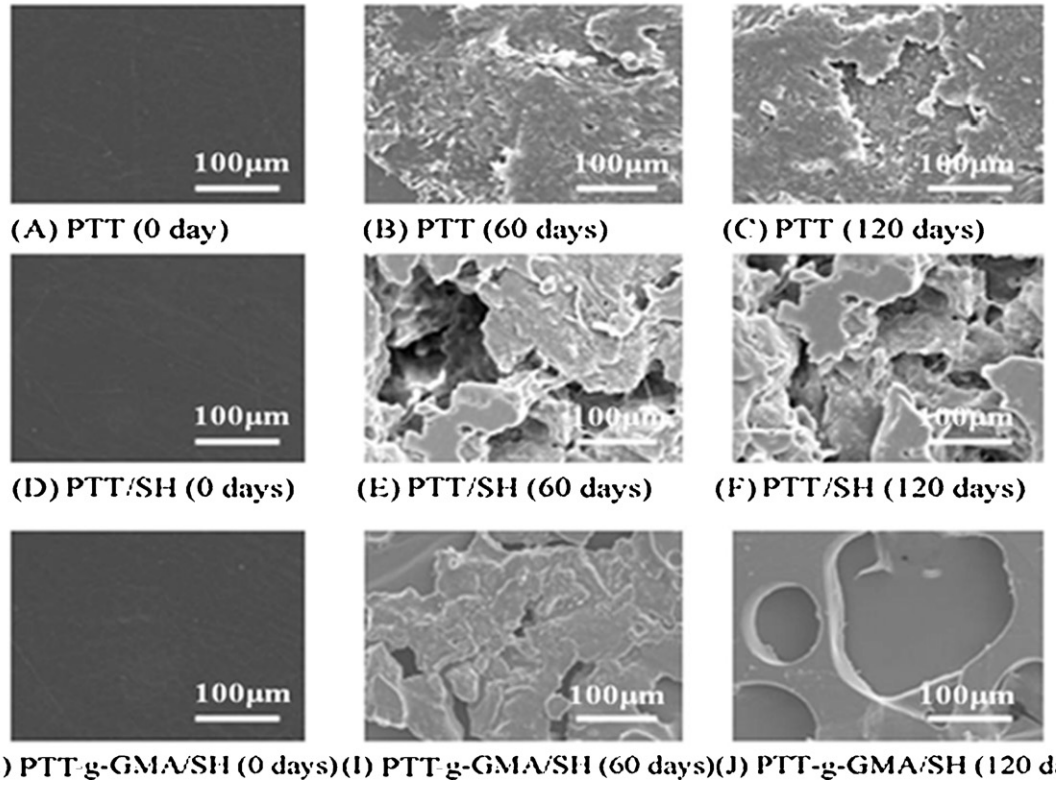

Fig. 6. SEM micrographs showing the morphology of PTT (A–C), PTT/SH (20 wt%) (D–F), and PTT-g-GMA/SH (20 wt%). (H–J) Films as a function of incubation time in soil. (K) Weight loss percentages of PTT, PTT-g-GMA, PTT/SH, and PTT-g-GMA/SH are shown as a function of incubation time in soil.

3.5. Water absorption of PTT and its composites

At the same SH content, the PTT-g-GMA/SH composites exhibited a higher resistance to water absorption than the PTT/SH composites (Fig. 5). The water resistance of the PTT-g-GMA/SH composites was moderate, and the hydrophobicity of SH was likely enhanced by interactions with the PTT-g-GMA. As expected, for both PTT/SH and PTT-g-GMA/SH, the percent water gain over the 60-day test period increased with SH content. Because the arrangement of polymer chains in these systems is random, this result could be attributable to both decreased chain mobility in composites with greater amounts of SH and to the hydrophilic character of SH, which weakly adheres to the more hydrophobic PTT.

3.6. Biodegradation of PTT and its composites

Changes in the morphology of both the PTT and PTT-g-GMA/SH composites were noted as a function of the amount of time they were buried in soil. SEM photomicrographs taken after 60 and 120 days illustrate the extent of morphological change (Fig. 6). PTT/SH composites (20 wt%; Fig. 6E and F) exhibited larger and deeper pits that appeared to be more randomly distributed than those in the PTT-g-GMA/SH (20 wt%) composites (Fig. 6I and J). These

analyses also indicated that biodegradation of the SH phase in PTT/SH (20 wt%) increased with time, confirming the results presented in Fig. 6K. After 60 days, the disruption of the PTT matrix became more obvious (Fig. 6B). This degradation was confirmed by increasing weight loss of the PTT matrix as a function of incubation time (Fig. 6K), which reached nearly 10% after only 120 days. The most likely cause of this weight loss was biodegradation. The SEM photomicrographs in Fig. 6 indicate that the PTT-g-GMA/SH (20 wt%) composites were more readily degraded than neat PTT. Moreover, at 60 and 120 days, larger pores were apparent in the PTT-g-GMA/SH composite (Fig. 6I and J), indicating a higher level of degradation. The rate of weight loss of the PTT-g-GMA/SH composites was also accelerated relative to that of PTT, exceeding 25% after 120 days (Fig. 6K). These results demonstrate that the addition of SH to the PTT-g-GMA enhanced the biodegradability of the composite.

Fig. 6K shows the percent weight change as a function of time for PTT/SH and PTT-g-GMA/SH composites buried in the soil compost. For both composites, the degree of weight loss increased with SH content. Composites with 40 wt% SH degraded rapidly over the first 60 days, losing a mass approximately equivalent to their SH content, and they showed a gradual decrease in weight over the next 60 days. PTT-g-GMA/SH exhibited a weight loss of approximately 3–9 wt%.

4. Conclusions

The biocompatibility and mechanical properties of SH composites with PTT and PTT-g-GMA were examined. FTIR and NMR analyses revealed the formation of condensation reactions between –OH groups in SH and glycidyl methacrylate groups in PTT-g-GMA, significantly altering the structure of the composite materials. The morphology of the PTT-g-GMA/SH composites was consistent with good adhesion between the SH phase and the PTT-g-GMA matrix. In mechanical tests, GMA grafting enhanced the mechanical properties of the composite, especially the tensile strength. PTT-g-GMA/SH exhibited a tensile strength of approximately 2–26 MPa more than PTT/SH. The cell viability tests indicated that PTT membranes have good biocompatibility for FBs to proliferate upon. The collagen secretion by FBs stimulated by PTT series membranes indicated the potential for PTT/SH membranes as biomaterials for tissue engineering. Although the water resistance of PTT-g-GMA/SH was higher than that of PTT/SH, the biodegradation rate of PTT-g-GMA/SH was lower than that of PTT/SH, but still higher than that of pure PTT, when incubated in soil. After 120 days, the PTT-g-GMA/SH (40 wt%) composite suffered greater than 60% weight loss. PTT/SH exhibited a weight loss of approximately 3–9 wt% more than PTT-g-GMA/SH. The degree of biodegradation increased with increasing SH content. Overall, the PTT-g-GMA/SH composites exhibited good mechanical properties, biocompatibility, and biodegradation. In the future, adjustment of the formula of this composite may be used to optimize its functionality and increase its product utility.

Acknowledgement

The authors thank the National Science Council (Taipei City, Taiwan, ROC) for financial support (NSC-101-2621-M-244-001).

References

Artemenko, A., Kylián, O., Choukourov, A., Gordeev, I., Petr, M., Vandrovcová, M., et al. (2012). Effect of sterilization procedures on properties of plasma polymers relevant to biomedical applications. *Thin Solid Films*, *520*, 7115–7124.

Brocchini, S. (2001). Combinatorial chemistry and biomedical polymer development. *Advanced Drug Delivery Reviews*, *53*, 123–130.

Cartier, H., & Hu, G.-H. (1998). Styrene-assisted melt free radical grafting of glycidyl methacrylate onto polypropylene. *Journal of Polymer Science: Part A: Polymer Chemistry*, *36*, 1053–1063.

Cho, K. Y., Eom, J.-Y., Kim, C.-H., & Park, J.-K. (2008). Grafting of glycidyl methacrylate onto high-density polyethylene with reaction. *Journal of Applied Polymer Science*, *108*, 1093–1099.

Golish, S. R., & Anderson, P. A. (2012). Bearing surfaces for total disc arthroplasty: Metal-on-metal versus metal-on-polyethylene and other biomaterials. *The Spine Journal*, *12*, 693–701.

Gupta, A., & Choudhary, V. (2012). Effect of multiwall carbon nanotubes on thermomechanical and electrical properties of poly(trimethylene terephthalate). *Journal of Applied Polymer Science*, *123*, 1548–1556.

Juntuek, P., Ruksakulpiwat, C., Chumsamrong, P., & Ruksakulpiwat, Y. (2011). Glycidyl methacrylate grafted natural rubber: Synthesis, characterization, and mechanical property. *Journal of Applied Polymer Science*, *122*, 3152–3159.

Kameda, T., Miyazawa, M., & Murase, S. (2005). Conformation of drawn poly(trimethylene terephthalate) studied by solid-state ^{13}C NMR. *Magnetic Resonance Chemistry*, *43*, 21–26.

Kim, J.-B., Chun, K.-W., Han, S.-K., & Kim, W.-K. (2010). Effect of human bone marrow stromal cell allograft on proliferation and collagen synthesis of diabetic fibroblasts *in vitro*. *Journal of Plastic Reconstructive and Aesthetic Surgery*, *63*, 1030–1035.

Kocer, H. B., Cerkez, I., Worley, S. D., Broughton, R. M., & Huang, T. S. (2011). Polymeric antimicrobial N-halamine epoxides. *ACS Applied Materials and Interfaces*, *3*, 2845–2850.

Kuan, C.-F., Ma, C.-C. M., Kuan, H.-C., Wu, H.-L., & Liao, Y.-M. (2006). Preparation and characterization of the novel water-crosslinked cellulose reinforced poly(butylene succinate) composites. *Composites Science and Technology*, *66*, 2231–2241.

Kuo, P.-C., Lin, M.-C., Chen, G.-F., Yiu, T.-J., & Tzen, J. T. C. (2011). Identification of methanol-soluble compounds in sesame and evaluation of antioxidant potential of its lignans. *Journal of Agricultural and Food Chemistry*, *59*, 3214–3219.

Lévesque, J., Hermawan, H., Dubé, D., & Mantovani, D. (2008). Design of a pseudo-physiological test bench specific to the development of biodegradable metallic biomaterials. *Acta Biomaterialia*, *4*, 284–295.

Liu, W., Mohanty, A. K., Drzal, L. T., Misra, M., Kurian, J. V., Miller, R. W., et al. (2005). Injection molded glass fiber reinforced poly(trimethylene terephthalate) composites: Fabrication and properties evaluation. *Industrial and Engineering Chemistry Research*, *44*, 857–862.

Marquès, E. F., Méndez, J. A., Gironès, J., Ginebra, M. P., & Pèlach, M. A. (2009). Evaluation of the influence of the addition of biodegradable polymer matrices in the formulation of self-curing polymer systems for biomedical purposes. *Acta Biomaterialia*, *5*, 2953–2962.

Mohdaly, A. A. A., Smetanska, I., Ramadanc, M. F., Sarhan, M. A., & Mahmoud, A. (2011). Antioxidant potential of sesame (*Sesamum indicum*) cake extract in stabilization of sunflower and soybean oils. *Industrial Crops and Products*, *34*, 952–959.

Muzzarellia, R. A. A., Grecoa, F., Busilacchia, A., Sollazzob, V., & Gigantea, A. (2012). Chitosan, hyaluronan and chondroitin sulfate in tissue engineering for cartilage regeneration: A review. *Carbohydrate Polymers*, *89*, 723–739.

Nair, L. S., & Laurencin, C. T. (2007). Biodegradable polymers as biomaterials. *Progress in Polymer Science*, *32*, 762–798.

Nyambo, C., Mohanty, A. K., & Misra, M. (2010). Polylactide-based renewable green composites from agricultural residues and their hybrids. *Biomacromolecules*, *11*, 1654–1660.

Safapour, S., Seyed-Esfahani, M., Auriemma, F., de Ballesteros, O. R., Vollaro, P., Girolamo, R. D., et al. (2010). Reactive blending as a tool for obtaining poly(ethylene terephthalate)-based engineering materials with tailored properties. *Polymer*, *51*, 4340–4350.

Sain, M., & Panthapulakkal, S. (2006). Bioprocess preparation of wheat straw fibers and their characterization. *Industrial Crops and Products*, *23*, 1–8.

Sell, S. A., McClure, M. J., Garg, K., Wolfe, P. S., & Bowlin, G. L. (2009). Electrospinning of collagen/biopolymers for regenerative medicine and cardiovascular tissue engineering. *Advanced Drug Delivery Reviews*, *61*, 1007–1019.

Shruti, N., & John, T. W. Y. (2011). Conductive polymer-based sensors for biomedical applications. *Biosensors and Bioelectronics*, *26*, 1825–1832.

Su, N.-W., Lin, Y.-L., Lee, M.-H., & Ho, C.-Y. (2005). Ankaflavin from monascus-fermented red rice exhibits selective cytotoxic effect and induces cell death on Hep G2 cells. *Journal of Agricultural and Food Chemistry*, *53*, 1949–1954.

Suja, K. P., Abraham, J. T., Thamizh, S. N., Jayalekshmy, A., & Arumughan, C. (2004). Antioxidant efficacy of sesame cake extract in vegetable oil protection. *Food Chemistry*, *84*, 393–400.

Suja, K. P., Jayalekshmy, A., & Arumughan, C. (2005). Antioxidant activity of sesame cake extract. *Food Chemistry*, *91*, 213–219.

Torres, N., Robin, J. J., & Boutevin, B. (2001). Functionalization of high-density polyethylene in the molten state by glycidyl methacrylate grafting. *Journal of Applied Polymer Science*, *81*, 581–590.

Toshikazu, K., Barbara, A. W., & Akio, T. (2012). Morphology, dynamic mechanical, and electrical properties of bio-based poly(trimethylene terephthalate) blends, part 2: Poly(trimethylene terephthalate)/poly(ether esteramide)/polycarbonate blends. *Journal of Applied Polymer Science*, *123*, 1056–1067.

Wong, K. J., Zahi, S., Low, K. O., & Lim, C. C. (2010). Fracture characterisation of short bamboo fibre reinforced polyester composites. *Materials and Design*, *31*, 4147–4154.

Wong, S., Shanks, R., & Hodzic, A. (2004). Interfacial improvements in poly(3-hydroxybutyrate)-flax fibre composites with hydrogen bonding additives. *Composites Science and Technology*, *64*, 1321–1330.

Wu, C. S. (2011). Performance and biodegradability of a maleated polyester bioplastic/recycled sugarcane bagasse system. *Journal of Applied Polymer Science*, *121*, 427–435.

Xuanyong, L., Chu, P. K., & Ding, C. (2010). Surface nano-functionalization of biomaterials. *Materials Science and Engineering R*, *70*, 275–302.

Yao, C., & Yang, G. (2010). Poly(trimethylene terephthalate)/silica nanocomposites prepared by dual *in situ* polymerization: Synthesis, morphology, crystallization behavior and mechanical properties. *Polymer International*, *59*, 492–500.

You, Z., Cao, H., Gao, J., Shin, P. H., Day, B. W., & Wang, Y. (2010). A functionalizable polyester with free hydroxyl groups and tunable physiochemical and biological properties. *Biomaterials*, *31*, 3129–3138.